Progress In Electromagnetics Research M, Vol. 115, 93–105, 2023

Thermoacoustic Imaging with Magnetic Nanoparticles under Envelope Short Pulse Alternating Magnetic Field Based on Magnetic Susceptibility Distribution Variation

Xingsheng Ni[1, 2], Hongjia Liu[1, 2], Yanhong Li[1, *], and Guoqiang Liu[1, 2, *]

Abstract—The magnetically mediated thermoacoustic imaging with magnetic nanoparticles (MNPs), which is excited by nonuniform pulsed envelope magnetic field, is constructed here, and the results of the magnetic susceptibility distribution of nanoparticles are extracted. In this paper, the theoretical model of the nonuniform magnetic field based on space-time separation is solved, and the Rosensweig model is used to obtain the heat generation of MNPs under the excitation of the pulsed envelope magnetic field. To solve the inverse problem, the heat source distribution is calculated by the time inversion method according to the sound pressure propagation formula under adiabatic conditions. After filtering out the effect of the nonuniform magnetic field, the magnetic susceptibility distribution can be obtained. The reconstruction results from simulation and experiment are consistent with the original distribution of MNPs and the distribution of the magnetic susceptibility. This method is expected to be applied to the precise diagnosis and treatment of tumors and provide a new idea for the precise localization and distribution image reconstruction of nanoparticles in vivo.

1. INTRODUCTION

Magnetic nanoparticles (MNPs) exhibit excellent heating effects under the action of an alternating magnetic field (AMF) owing to their hysteresis [1] and relaxation [2] phenomena. Both phenomena are closely related to the particle size of MNPs. At the superparamagnetic domain size, Brownian relaxation and Néel relaxation replace hysteresis as the primary heating factors [3]. After decades of research, the heating effect of the MNPs has been widely applied in medicine, materials, and industry [4–6]. Owing to their good biocompatibility, MNPs have great development potential in tumor therapy [7] and drug delivery [8]. Therefore, imaging methods suitable for monitoring MNPs are urgently required in order to accurately guide MNPs to the target site [9, 10].

Superparamagnetic nanoparticles such as iron oxide show great potential for photoacoustic (PA) [11] and thermoacoustic (TA) [12] imaging methods. These two methods are similar in that they both use the acquired ultrasound signals to reconstruct the target, which has the advantage of high resolution ultrasound imaging. For PA, short lasers are typically utilized to excite the thermal effects and mechanical motions of MNPs, which in turn generate ultrasonic signals. For TA, radio frequency magnetic fields are used to excite ultrasonic signals from biological tissues and MNPs. Microwave induced thermoacoustic imaging (MITAI) [13] and magnetically mediated thermoacoustic imaging (MMTAI) [14] are two main TA imaging methods. The generation mechanisms of thermoacoustic sources of these two methods are different. MITAI relies on the enhanced absorption of radiation energy by the medium, and MNPs are used as contrast agents to improve the contrast of the reconstructed

Received 20 December 2022, Accepted 3 February 2023, Scheduled 21 February 2023
* Corresponding author: Yanhong Li (liyanhong@mail.iee.ac.cn), Guoqiang Liu (liuguoqiang@mail.iee.ac.cn).
[1] Institute of Electrical Engineering Chinese Academy of Sciences, Beijing 100190, China. [2] University of Chinese Academy of Sciences, Beijing 100049, China.

image [15]. In contrast, MMTAI uses magnetic relaxation loss to absorb energy from a non-radiating magnetic field, and the permeability of MNPs is the key to the magnetothermal effect and TA signal intensity. In addition, MMTAI can also take advantage of the unique magnetic modulation capability of MNPs under the action of an external AMF to enhance the imaging contrast through differential imaging, thereby eliminating the limitations of thermoacoustic signals generated by surface biological tissues [16]. Furthermore, the frequency of MITAI which reaches hundreds of MHz and even GHz, limits the imaging depth. To improve the imaging depth and optimize the excitation mode, near-field thermoacoustic imaging (100 MHz) has been proposed by scholars, and then the excitation frequency has been further reduced by Piao et al. [12] and Feng et al. [14]. The frequency of MITAI is dozens of times of MMTAI, so the penetration depth of MITAI is much lower than that of MMTAI. Therefore, compared to MITAI, MMTAI has a higher detection depth and better application prospects.

In this paper, based on the MMTAI, a low-frequency pulsed envelope magnetic field is used to stimulate MNPs to generate a stable TA signal. The pulsed envelope magnetic field has a width of 1 µs which is generated by tightly wound coils. Under the action of a magnetic field, Brownian and Néel relaxations of MNPs induce magnetothermal effect and further excite ultrasonic signals. The generation of the thermal source and ultrasound signal is related to the magnetic susceptibility of the MNPs. Therefore, the magnetic susceptibility of MNPs can be obtained using the collected ultrasound signals to generate a distribution image. In theory, the method of space-time separation is used to solve the forward problem of the electromagnetic field. For the inverse problem, Green's function and time inversion method are used to solve the thermal source distribution from the sound pressure wave equation. To verify the theoretical analysis, a simulation model of magnetic susceptibility based on MNPs is established. The magnetic field distribution of the pulse envelope and the formation process of the TA wave were analyzed. In the experiment, a verification system with the same scale as that of the simulation was conducted. TA signals were acquired using an ultrasonic transducer, and the B-scan image along the Y-axis was reconstructed. Then, the magnetic susceptibility distribution image was constructed according to the corresponding relationship between the magnetic susceptibility of the MNPs and the distribution of the heat sources. Both simulations and experiments verified that the magnetic susceptibility parameters of MNPs can be extracted from the TA signals generated by the pulse envelope magnetic field excitation. The method presented in this paper provides a new idea for the magnetic susceptibility characterization and imaging of MNPs.

2. PRINCIPLE AND METHOD

2.1. Theoretical Model

As shown in Figure 1, the short time pulse envelope current $\mathbf{J}_e(\mathbf{r}, t)$ is passed through the tightly wound coil to excite a nonuniform pulsed magnetic field. The MNPs as imaging targets are excited by a

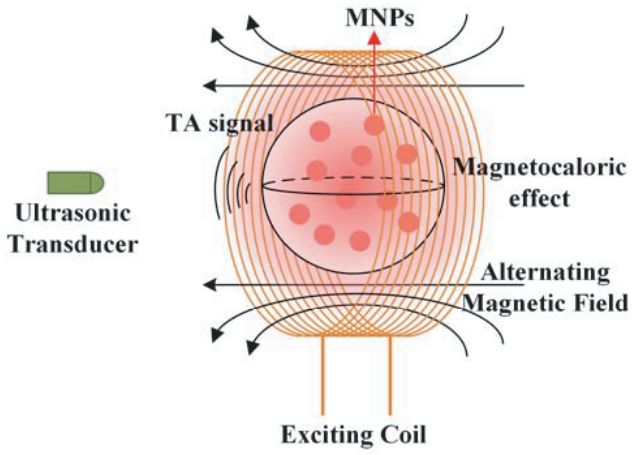

Figure 1. Theoretical schematic.

magnetic field to generate TA signals, which are received by the ultrasound transducer. According to the magnetic susceptibility information of MNPs carried by the TA signal, the distribution image can be reconstructed. The excitation current flowing in the coil can be considered uniform and is denoted by $\mathbf{J}_e(\mathbf{r})g(t)$. As a typical transient field solution problem, since the solution region concerned is the non-eddy current region, the vector magnetic potential can be solved using the vector Poisson equation.

Since the conductivity of the biological tissue is almost zero [17], the secondary magnetic field generated by the eddy current is much smaller than the primary magnetic field generated by the excitation current, which can be ignored. After ignoring the secondary magnetic field, according to the magnetization characteristics of magnetic materials, the magnetic field constitutive relation of the region where the MNPs are located can be expressed as

$$\mathbf{H}(\mathbf{r},t) = \frac{1}{\mu_0(1+\chi)}\mathbf{B}(\mathbf{r},t) \approx \frac{1}{\mu_0(1+\chi)}\mathbf{B}_1(\mathbf{r},t) \tag{1}$$

where χ is the magnetic susceptibility of the MNPs, and μ_0 is the permeability of vacuum. Under the action of excitation current, the time term of the magnetic field strength is expressed as $g(t)$. The vector magnetic potential $\mathbf{A}_1(\mathbf{r},t)$ is introduced according to the Gauss magnetic field theorem.

$$\mathbf{B}_1(\mathbf{r},t) = \nabla \times \mathbf{A}_1(\mathbf{r},t) \tag{2}$$

The MNPs have little electrical conductivity, and the eddy current is not generated. In the non-eddy current region, according to Ampere's law, the vector Poisson equation with the time term eliminated corresponding to this area is as follows.

$$\nabla \times \left[\frac{1}{\mu_0(1+\chi)}\nabla \times \mathbf{A}_1(\mathbf{r})\right] - \nabla\left[\frac{1}{\mu_0(1+\chi)}\nabla \cdot \mathbf{A}_1(\mathbf{r})\right] = 0 \tag{3}$$

The boundary conditions must be given to solve the vector Poisson equation. Therefore, in addition to the field equation in the nanoparticle region, the field equations of the tissue and coil should also be considered. Since the influence of the secondary magnetic field generated by the eddy current in the tissue is ignored, the field equation of tissue and coil can be combined.

$$\nabla \times \left[\frac{1}{\mu_0}\nabla \times \mathbf{A}_1(\mathbf{r})\right] - \nabla\left[\frac{1}{\mu_0}\nabla \cdot \mathbf{A}_1(\mathbf{r})\right] = \mathbf{J}_e(\mathbf{r}) \tag{4}$$

After eliminating the time term, the inner boundary S condition of the entire solution space can be expressed as follows.

$$\begin{cases} \mathbf{A}_{nps}(\mathbf{r})|_S = \mathbf{A}_{exc}(\mathbf{r})|_S \\ \dfrac{1}{\mu_0(1+\chi)}\,\mathbf{n} \times \nabla \times \mathbf{A}_{nps}(\mathbf{r})|_S = \dfrac{1}{\mu_0}\,\mathbf{n} \times \nabla \times \mathbf{A}_{exc}(\mathbf{r})|_S \end{cases} \tag{5}$$

To ensure the integrity and uniqueness of the solution, the external boundary conditions of the corresponding solution space must be supplemented

$$\begin{cases} \mathbf{n} \cdot \mathbf{A}_{exc}(\mathbf{r})|_\infty = 0 \\ \mathbf{n} \times \mathbf{A}_{exc}(\mathbf{r})|_\infty = 0 \end{cases} \tag{6}$$

During the introduction of the field potential equation, each physical quantity is separated into time and space. This process transforms the problem of solving the transient magnetic field into that of solving the space and time terms of the vector potential. Through numerical simulation, the spatial term of the physical quantity can be obtained. Finally, the spatial distribution of each physical quantity is multiplied by the corresponding time term to obtain a complete result.

The pulse envelope magnetic field has a short action time (1 µs), so the characteristics of the biological tissue itself determine that the dielectric loss and Jouleheat can be ignored [18] in the presence of magnetic nanoparticles. Only the magnetization energy increment of MNPs under the action of magnetic field is considered

$$\frac{\mathrm{d}W(\mathbf{r},t)}{\mathrm{d}t} = \mu_0 H(\mathbf{r},t)\frac{\mathrm{d}M(\mathbf{r},t)}{\mathrm{d}t} \tag{7}$$

The time term of the excitation magnetic field is a pulsed signal composed of multiple cycles of AMF. Considering the effect of the periodic part, the magnetization energy increment is mainly

produced by Brownian relaxation and Néel relaxation, which leads to local heating of MNPs. In this process, the heat function generated by MNPs can be expressed as [19]

$$Q\left(\mathbf{r},t\right)=\frac{N}{2}\mu_0\chi_0H^2(\mathbf{r})\frac{\omega_0^2\tau}{1+(\omega_0\tau)^2}g(t) \tag{8}$$

where ω_0 is the frequency of the AMF; N is the number of action cycles of the AMF in the pulse time; χ_0 and τ are the magnetic susceptibility and relaxation time of the MNPs, respectively. For an instantaneous pulsed magnetic field, the time function $g(t)$ is equivalent to the impulse function $\delta(t)$.

After the MNPs were heated instantaneously, TA waves were generated due to the thermal expansion. Due to thermal constraints, the thermal diffusion of MNPs can be neglected in a short time by considering only the acoustic wave equation [20], which can be approximately expressed as follows.

$$\left(\nabla^2-\frac{1}{c^2}\frac{\partial^2}{\partial t^2}\right)p\left(\mathbf{r},t\right)=-\frac{\beta}{C_p}\frac{\partial}{\partial t}Q(\mathbf{r},t) \tag{9}$$

where $p(\mathbf{r},t)$ is the acoustic pressure, c the acoustic velocity of the ultrasonic waves, C_p the constant pressure specific heat capacity, and β the thermal expansion coefficient. The ultrasonic signal is excited by the thermal sound source of MNPs, which can be solved by Green's function method [21] under linear acoustic theory during the numerical analysis and can be actually received by the ultrasonic transducer. To reconstruct the magnetic susceptibility distribution of MNPs, it is necessary to reconstruct the heat source distribution from the TA signal. The time inversion algorithm is usually used for inverse source analysis, and the expression of the reconstructed heat absorption distribution in the acoustic source term is [22]

$$Q(\mathbf{r}')\approx-\frac{C_p}{2\pi c^3\beta}\oint dS_d\frac{\mathbf{n}\cdot(\mathbf{r}-\mathbf{r}')}{R^2}\frac{\partial}{\partial t}p(\mathbf{r},R/c) \tag{10}$$

where $\mathbf{r}'$ denotes the point at which the MNPs are located inside the tissue, $\mathbf{r}$ the position of the receiving ultrasonic transducer, S_d the acoustic radiation surface of the ultrasonic transducer, $\mathbf{n}$ the normal direction of $\mathbf{r}$ position on S_d, and $R=|\mathbf{r}-\mathbf{r}'|$ the positional difference between the ultrasonic transducer and MNPs. After reconstructing the source term, the magnetic susceptibility of the MNPs is further reconstructed.

In order to solve the electromagnetic field inverse problem, the objective function can be built

$$\xi=\left\|Q_r(\mathbf{r}')-Q_c(\mathbf{r}')\right\|_2^2 \tag{11}$$

where $Q_r(\mathbf{r}')$ is obtained by the sound field inverse problem, based on Equation (10), using the measured acoustic pressure data, and $Q_c(\mathbf{r}')$ can be obtained by Equation (8) when the initial value of magnetic susceptibility is given. The objective function can be solved using an iterative optimization method, and the magnetic susceptibility can be reconstructed using the least squares method.

2.2. Numerical Simulation

In this section a three-dimensional geometric model is established to analyze the thermoacoustic excitation process and sound field distribution characteristics of MNPs under the action of the envelope short pulse alternating magnetic field. The components of the simulation model are shown in Figure 2.

The outermost phantom is used to simulate normal biological tissue, and its length, width, and height are 5 cm, 3 cm, and 3 cm, respectively, and its geometric center is located at the origin. According to the biological tissue characteristic parameters given in the literature [23, 24], the relative magnetic permeability and conductivity are set to 1 and 0.2 S/m, respectively. The magnetic fluid solution is placed in a cuboid with dimensions of 1 cm × 4 mm × 2.5 cm at the center of the phantom. The parameters of MNPs used in the simulation are listed in Table 1. The phantom with the magnetic fluid solution is placed in a coil with a radius of 2.2 cm. The center of the coil coincides with that of the phantom. An alternating current with an amplitude of 10 A and duration of 1 μs flows through the coil, and the frequency of the alternating current is 10 MHz during the duration.

According to the theory, the magnetic field distribution of the model needs to be solved to obtain an endothermic distribution of the MNPs. The spatial magnetic field distribution of any fault surface

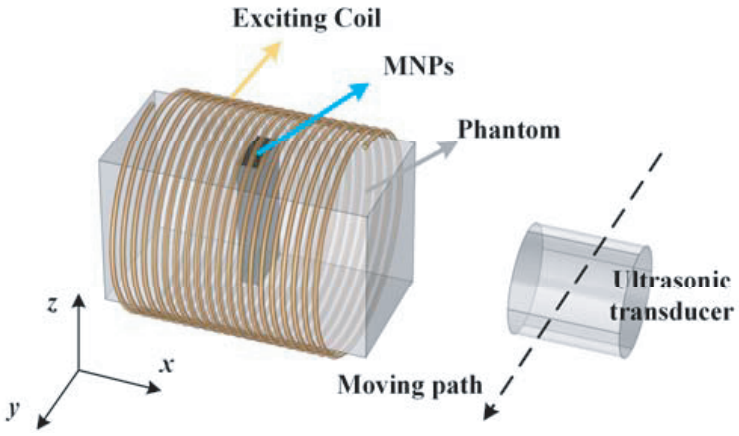

Figure 2. Components of the simulation model and their spatial relationships.

Table 1. Specific parameter of magnetic nanoparticles (MNPs) for simulation [25].

Symbol	Parameters	Value
R	average particle size	10 nm
σ_d	Size deviation	± 2 nm
M_d	Saturation magnetization	$446\,\mathrm{kAm^{-1}}$
ρ_M	Density of MNPs	$5180\,\mathrm{kgm^{-3}}$
C_M	Specific heat capacity of MNPs	$670\,\mathrm{Jkg^{-1}K^{-1}}$
C_P	Specific heat of carrier fluid	$2080\,\mathrm{Jkg^{-1}K^{-1}}$
η	Viscosity coefficient of carrier fluid	$2.35 \times 10^{-3}\,\mathrm{kgm^{-1}s^{-1}}$
T	Simulated ambient temperature	293 K
K	Anisotropy constants of MNPs	$23\,\mathrm{kJm^{-3}}$
β	Coefficient of thermal expansion	$7 \times 10^{-4}\,\mathrm{K^{-1}}$

at any time can be extracted, and then the heat source distribution of the corresponding surface can be obtained using Equation (8). The normalized distributions of the magnetic field and heat source on the fault surface $z = 0$ at $t = 0.5\,\mu$s are shown in Figure 3, respectively. The magnetic field and heat source distribution at any time during the entire action time can be deduced from the results at this time with the time item of the pulse envelope excitation current. It can be seen from Figure 3 that the primary magnetic field generated by the coil is approximately uniform at the center position. The nonuniform distribution of magnetization generated by nanoparticles causes the magnetic field in the central region to exhibit a trend of high on both sides and low in the middle. Because the magnetic susceptibility and electrical conductivity of biological tissues are quite small, the heat generated by them is directly ignored during the simulation. Figure 3 shows the thermoacoustic source distribution of MNPs, which changes abruptly at the boundary between the nanoparticle and the phantom. It shows that the distribution of the thermoacoustic source varies with magnetic susceptibility. In general, a thermoacoustic source is affected by the nonuniform distribution of magnetic susceptibility and the corresponding nonuniform magnetic field distribution of the magnetic nanoparticles.

For the acoustic pressure signal generated by the magnetization energy of MNPs as the heat source, the forward modeling problem of the sound field is solved using Equation (8). As shown in Figure 4, the normalized nephogram of the acoustic pressure on the fault surface $z = 0$ at $t = 0.5\,\mu$s is extracted. On this fault surface, a two-dimensional intercept line is selected, and its endpoint coordinates are $(-1.5, 0)$ cm and $(1.5, 0)$ cm, respectively. The normalized distributions of the magnetic susceptibility

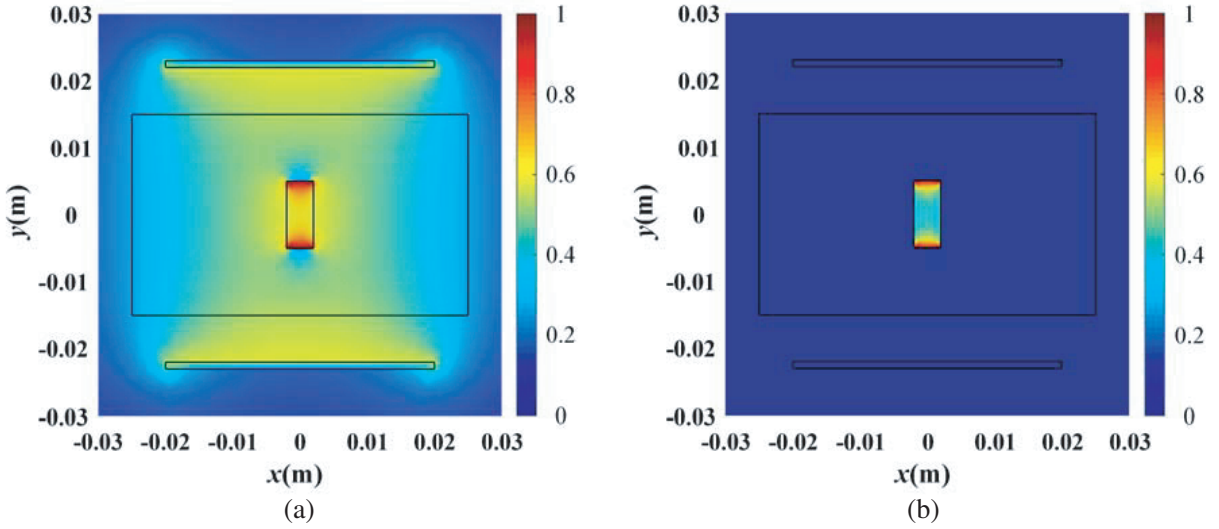

Figure 3. Normalized distribution at 0.5 μs on fault plane. (a) The magnetic field and (b) the thermoacoustic source.

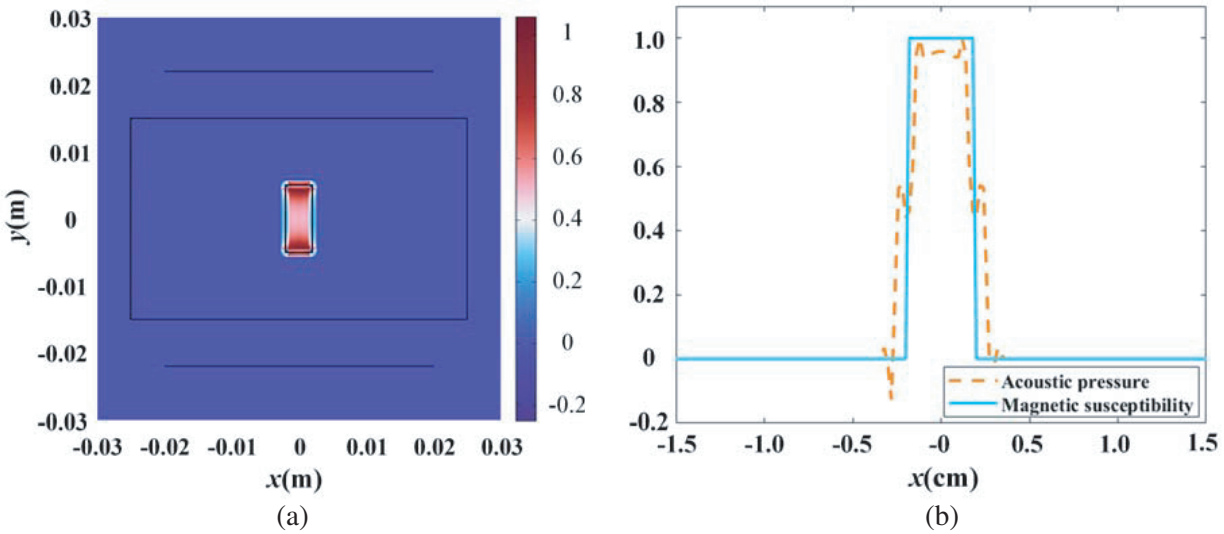

Figure 4. Normalized distribution of (a) the acoustic pressure distribution and (b) the changing curve of acoustic pressure with magnetic susceptibility at 0.5 μs on fault surface $z = 0$.

and acoustic pressure are shown in Figure 4. This indicates that the acoustic pressure undergoes abrupt changes and fluctuations at the boundary of the magnetic susceptibility variation. During the action of the excitation current, the boundary variation characteristics of the distribution of the heat source, acoustic pressure, and magnetic susceptibility of MNPs are basically consistent.

After solving the acoustic source distribution, an analog ultrasonic transducer with a center frequency of 2.25 MHz is located at the $(2, 0)$ cm point to receive the acoustic pressure signal. The time-domain and frequency-domain characteristics of the transducer are shown in Figure 5. The line connecting the ultrasonic transducer placement position and the central point of the MNPs region is on the fault surface $z = 0$ and intersects with each boundary of the magnetic susceptibility change. In the period from 0 μs to 30 μs, the normalized result of the acoustic pressure signal received by the ultrasonic transducer is shown in Figure 5.

The signal actually received by the ultrasound transducer is the convolution of the acoustic pressure

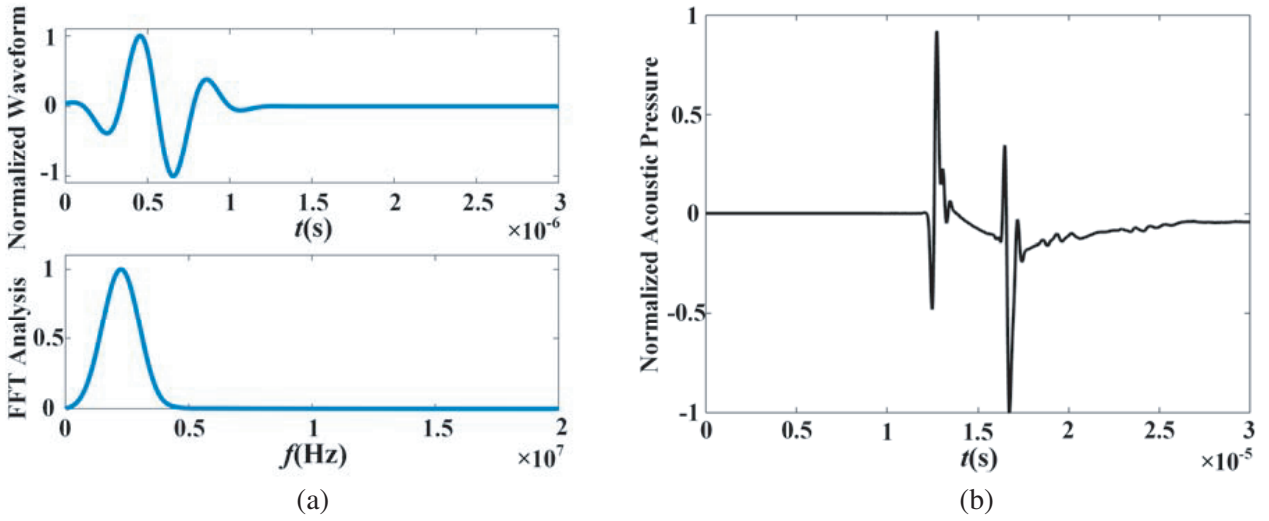

Figure 5. (a) Impulse response and frequency response of ultrasonic transducer. (b) Simulated normalized thermoacoustic signal received by ultrasonic transducer.

signal and the characteristics of the transducer. Because the speed of sound in biological tissue is approximately 1500 m/s, the theoretical times for the acoustic wave to propagate from the two boundaries to the transducer location are 12 µs and 16 µs, respectively. In Figure 5, the numerical simulation results are about 12.7 µs and 16.7 µs. This deviation is introduced by the equivalence of the thermal expansion coefficient of the MNPs and the specific heat of the ferrofluid solution, but the accuracy of the numerical simulation analysis is preliminarily verified.

According to the numerical simulation analysis, the magnetic susceptibility of MNPs and the distribution characteristics of the external magnetic field determine the distribution characteristics of the heat source. However, when the geometric parameters of the coil and excitation current are known, the distribution of the magnetic field can be solved accurately, thereby eliminating its influence on the distribution of the heat source. When the magnetic field distribution is known, the magnetic susceptibility distribution of the MNPs determines the distribution of the thermoacoustic source and sound pressure. With the acoustic pressure data of the forward problem collected by the numerical simulation, the heat source distribution can be reconstructed using Equation (10) based on the time

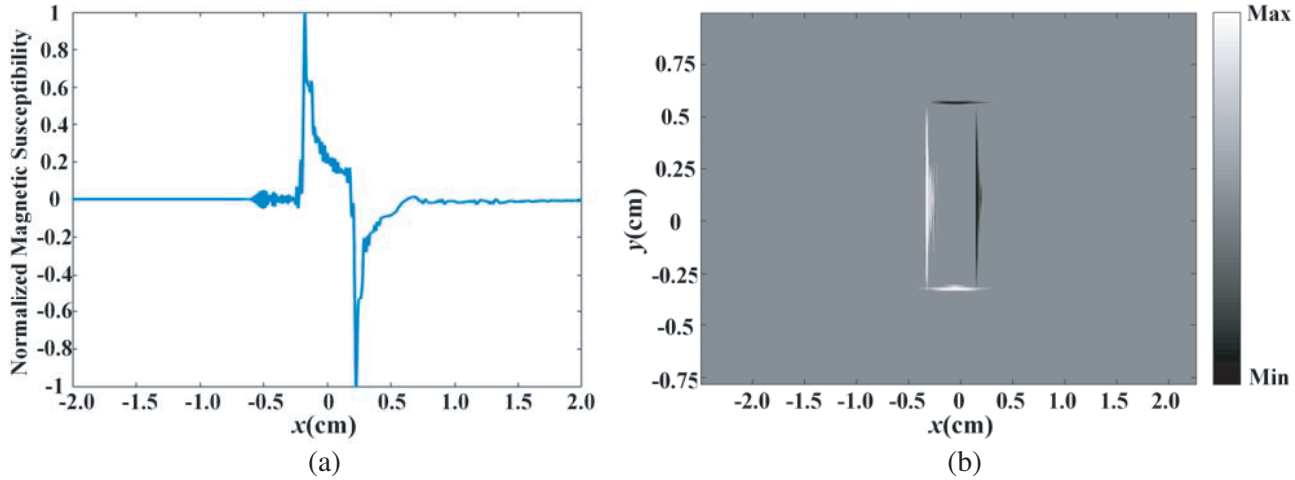

Figure 6. (a) Normalized inversion result of magnetic susceptibility. (b) Normalized image by B-scan.

reversal method. Combined with Equation (11), the least squares method is used to reconstruct the magnetic susceptibility change corresponding to Figure 5, as shown in Figure 6. Based on the position of the ultrasonic transducer, the magnetic susceptibility abruptly changes upward at 1.8 cm and downward at 2.2 cm, which is consistent with the simulation model structure. To invert the magnetic susceptibility distribution image, a total of 602 acquisition points are arranged. All acquisition points are arranged at equal intervals of 0.1 mm. 401 points are set at -1 cm to 1 cm in the X-axis direction, and 201 points are set at -2 cm to 2 cm in the Y-axis direction. The acoustic pressure signals of all the acquisition points are extracted by numerical simulation, and the normalized image is reconstructed with the collected data, as shown in Figure 6. Compared with the simulation model, the reconstructed image clearly reflects the magnetic susceptibility distribution characteristics, which is consistent with the boundaries of the nanoparticle region. It is proven that the magnetic susceptibility distribution characteristics of MNPs can be inverted from the sound pressure signal with the magnetic field distribution.

3. EXPERIMENTAL VERIFICATION

The schematic diagram of the experiment system is shown in Figure 7. The system is divided into three parts: magnetic field generation, coupling conversion from the electromagnetic field to the acoustic field, and acoustic signal acquisition. The magnetic field generation part consists of a waveform generator, an RF power amplifier, and an LC parallel resonant circuit. The resonance frequency of the resonant circuit (coil with capacitor network) is fixed at 9.8 MHz, and the measured quality factor is approximately 20. The number of turns of the tightly wound coil is 21; radius is 2 cm; and inductance is 16.42 μH. This coil is placed in insulating oil, and its thermal effect is negligible. The capacitance of capacitor C1 is 15 μF which forms a parallel resonance with the coil. Capacitor C2 and resistor R are connected in series with the branch where the coil is located to reduce the fall time of the pulse envelope current and signal tailing. Their values are 45 μF and 6 Ω, respectively. A current monitor is used to detect the current flowing through the coil to distinguish the form of the magnetic field and operating state of the coil.

The phantom is immersed in a tank filled with insulating oil and placed at the center of the coil.

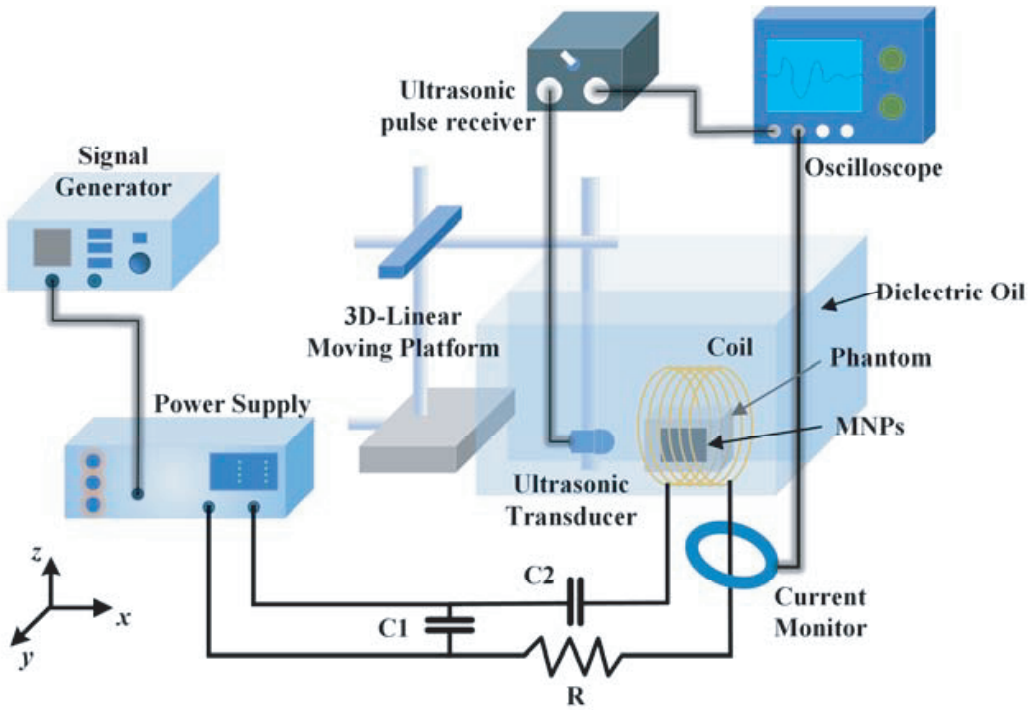

Figure 7. Schematic diagram of the experiment system.

Insulating oil can be used as an ultrasonic coupling agent. A waveform generator is used to generate a 1 μs burst signal with a frequency of 9.8 MHz as shown in Figure 9. After the signal is fed into the RF power amplifier, the single peak amplitude of the pulse envelope current in the excitation coil reaches 3.76 A, which excites MNPs to generate thermoacoustic signal. An ultrasonic transducer is used to receive the thermoacoustic signal, and its center frequency is 2.25 MHz. The detected signal is fed into the ultrasonic pulse receiver with an amplification of 50 dB. Finally, an oscilloscope is used to collect the signal from the output of the ultrasonic pulse receiver, and the average number of data is 1024.

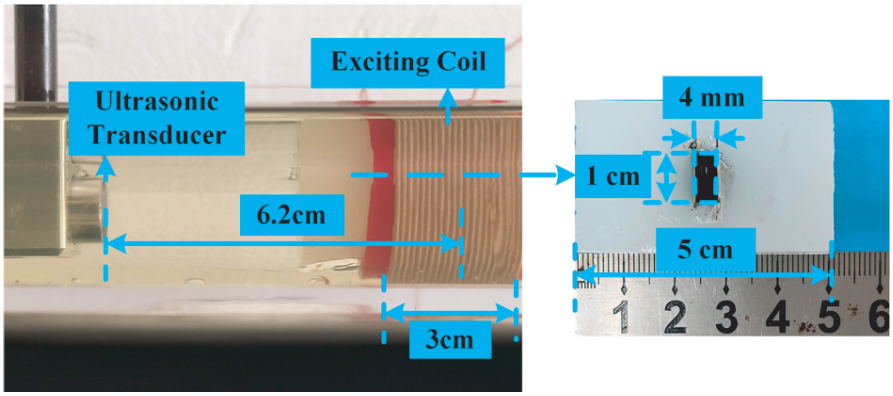

Figure 8. Picture of an experimental phantom with MNPs.

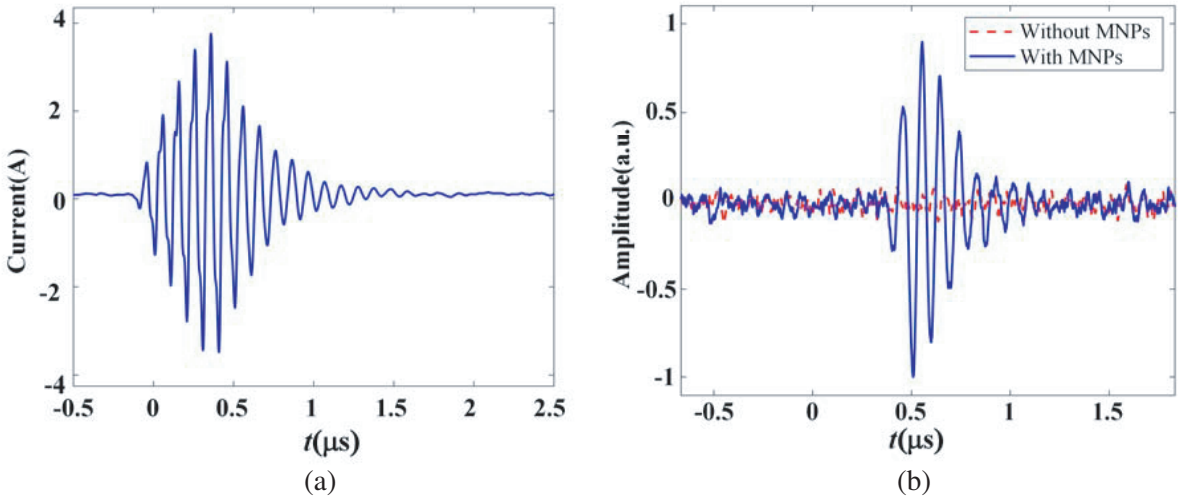

Figure 9. (a) Excitation current. (b) The thermoacoustic signal collected by the ultrasonic probe after normalization.

As shown in Figure 8, MNPs with an average radius of 10 nm are placed in a 4 mm wide gap at the center of the phantom. The ultrasonic transducer is placed 6.2 cm from the first interface of the gap. Figure 9 shows the thermoacoustic signals received by the ultrasonic transducer with and without the MNPs. The thermoacoustic signal disappears after the MNPs-containing phantom is removed. To facilitate comparison, normalization is performed. Theoretically, the acoustic velocity of ultrasonic waves in oil is approximately 1520 m/s [26], and it takes 40.78 μs for the probe to receive the signal from the first interface between the phantom and the MNPs. However, due to the existence of hardware delay and measurement error, the time of the wave cluster corresponding to the first boundary received by the ultrasonic transducer is 41.42 μs, which is slightly delayed from the theory.

To obtain B-scan imaging of the MNPs, a three-dimensional linear motion platform is used to control the translation of the ultrasonic transducer in the Y-axis direction, and each translation is 0.5 mm. A total of 40 groups of signals are collected as the raw data. Due to the systematic error, the measured data are preliminarily processed, including DC component removal and normalization. To reconstruct the distribution of MNPs more accurately, an image processing method based on wavelet transform is used to process the data obtained in the Y-axis direction. The obtained result is presented in Figure 10. The reconstructed image reflecting the magnetic susceptibility distribution of MNPs is basically consistent with the actual location of the nanoparticles (red box). Since the ultrasonic transducer is non-focused, it also receives a thermoacoustic signal when the central position of the transducer is not aligned with the MNPs. The motion path of the ultrasonic transducer cannot be completely guaranteed to be in a straight line, which changes the peak position of the acoustic signal received at different acquisition points. Meanwhile, only one-way scanning is performed, the redundant signals are not eliminated when compiling the inversion algorithm. The existence of these causes creates artifacts in the final result.

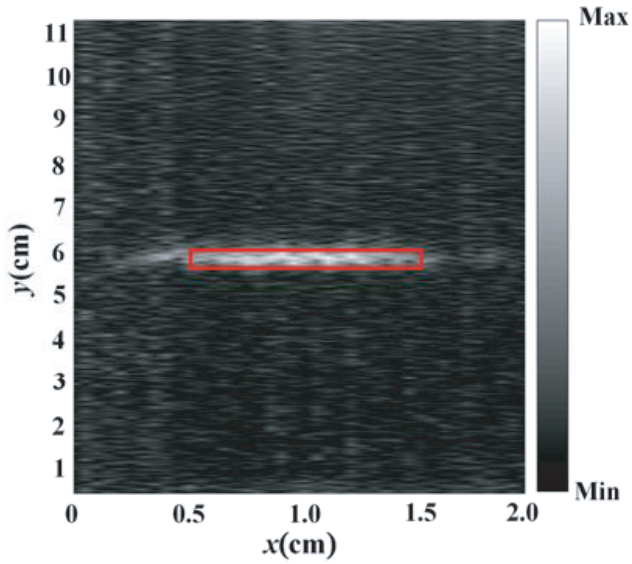

Figure 10. Image reconstruction result.

4. DISCUSSION

This paper explains the mechanism of TA signal generation from MNPs excited by a pulse envelope current. A method that reflects the magnetic susceptibility distribution of MNPs based on received acoustic signals is deduced. A simulation model and an experimental system are constructed to verify the results of the theoretical analysis. In the numerical simulation, the magnetic field distribution inside the coil under the excitation of the pulse envelope current is obtained. Then, the sound pressure distribution of MNPs under the action of a pulsed envelope magnetic field is explored, which provides a basis for the determination of experimental system parameters and experimental analysis. A resonant network with a resonance frequency of 9.8 MHz is designed, and a corresponding experimental system is built. A gel phantom with a slit in the center is used to simulate biological tissue, and MNPs are added into the slit, then the TA signal is collected using the experimental system. Finally, the magnetic susceptibility distribution characteristics of the MNPs are obtained by simulation and experiment. It provides a more accurate analysis method for further exploratory research and a data basis for the development of therapeutic applications.

As shown in Figure 11, the spectrum of the data is obtained through a Fast Fourier Transform (FFT). The main peak of the frequency distribution of the TA signal collected in the experiment is located at 1.8 MHz. The TA signal includes the frequency characteristic which is covered by the

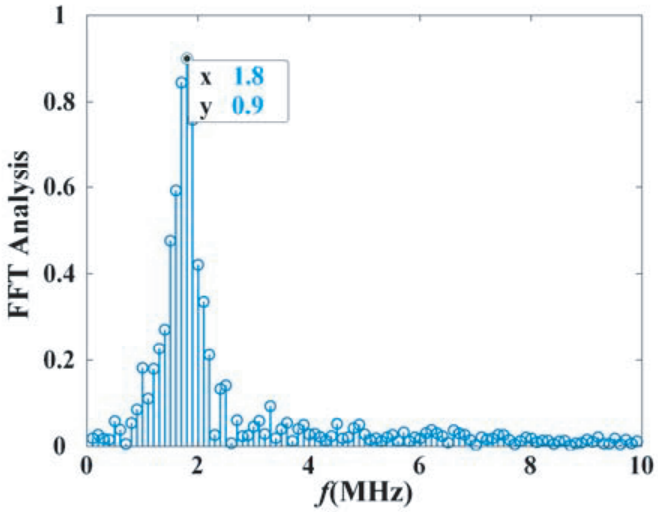

Figure 11. Spectral analysis of Fast Fourier Transform of TA signal.

ultrasonic transducer with the main frequency of 2.25 MHz. The two closer frequencies widen the main peak range of the heat signal, thereby affecting the imaging contrast. Furthermore, since the frequency of the excitation signal is 9.8 MHz, its penetration depth is approximately 21 cm. Compared with microwave thermoacoustic and near-field thermoacoustic imaging, the detection depth is significantly improved which can meet the requirements of many scenarios. Considering the safety of MNPs and the tolerance of the human body, the concentration of magnetic nanoparticles should be reduced as much as possible. However, under the same excitation conditions, the amplitude of the TA signal decreases with the decrease of MNPs concentration until it becomes undetectable. To achieve TA signal detection at low MNPs concentrations, it is necessary to further improve the sensitivity of the detection device and the strength of the excitation magnetic field, or to improve the characteristics of the MNPs themselves.

In future research, it is expected to improve the quality of the TA signal by increasing the power of the amplifier and reducing the harmonics in the excitation signal. For biological imaging methods, in addition to the single-direction signal acquisition, signal acquisition in different dimensions should be added. In addition, digital image filtering and fusion methods can be considered to improve the image quality and imaging speed.

5. CONCLUSION

In this paper, we have analyzed the theory of magnetically mediated thermoacoustic imaging with MNPs under pulse envelope excitation. The feasibility of TA imaging with MNPs under an envelope short pulse alternating magnetic field based on magnetic susceptibility distribution variation was verified by simulation and experiment. A comprehensive simulation model with a tightly wound coil and MNPs was established. The magnetic field and acoustic pressure distribution of MNPs excited by the pulse envelope current were simulated and analyzed to verify the generation of the TA signal. The coil and phantom were fabricated, and a cross-sectional reconstructed image reflecting the changes in the magnetic susceptibility distribution of MNPs was experimentally obtained. Although there are many challenges to be solved for application in human body of the TA imaging with low concentration MNPs, we still believe that with advances in nanoscience and signal processing, there is great potential for real-time tracking and imaging using MNPs in vivo.

ACKNOWLEDGMENT

This work was supported by the Natural Science Foundation of Beijing under Grant No. 7212209, National Natural Science Foundation of China under Grant No. 52277233, National Major Scientific

Research Instrument Development Project under Grant No. 62027901, Chinese Academy of Sciences under Grant No. YJKYYQ20190005, and the National Natural Science Foundation of China under Grant No. 51937010.

REFERENCES

1. Hiergeist, R., W. Andrä, N. Buske, R. Hergt, I. Hilger, U. Richter, and W. Kaiser, "Application of magnetite ferrofluids for hyperthermia," *J. Magn. Magn. Mater.*, Vol. 201, No. 1, 420–422, 1999.
2. Hergt, R., W. Andra, C. G. d'Ambly, I. Hilger, W. A. Kaiser, U. Richter, and H. G. Schmidt, "Physical limits of hyperthermia using magnetite fine particles," *IEEE Trans. Magn.*, Vol. 34, No. 5, 3745–3754, 1998.
3. Carrey, J., B. Mehdaoui, and M. Respaud, "Simple models for dynamic hysteresis loop calculations of magnetic single-domain nanoparticles: Application to magnetic hyperthermia optimization," *J. Appl. Phys.*, Vol. 109, 083921, 2011.
4. Chen, R., G. Romero, M. G. Christiansen, A. Mohr, and P. Anikeeva, "Wireless magnetothermal deep brain stimulation," *Science*, Vol. 347, 6229, 1477–1480, 2015.
5. Wang, H., S. C. Zhao, J. Zhou, K. P. Zhu, X. Cui, W. H. Huang, M. N. Rahaman, C. Q. Zhang, D. P. Wang, "Biocompatibility and osteogenic capacity of borosilicate bioactive glass scaffolds loaded with Fe_3O_4 magnetic nanoparticles," *J. Mater. Chem. B*, Vol. 3, No. 21, 4377–4387, 2015.
6. Beck, M. M., C. Lammel, and B. Gleich, "Improving heat generation of magnetic nanoparticles by pre-orientation of particles in a static three tesla magnetic field," *J. Magn. Magn. Mater.*, Vol. 427, 195–199, 2017.
7. Dutz, S. and R. Hergt, "Magnetic nanoparticle heating and heat transfer on a microscale: Basic principles, realities and physical limitations of hyperthermia for tumour therapy," *Int. J. Hyperther.*, Vol. 29, No. 8, 790–800, 2013.
8. Mura, S., J. Nicolas, and P. Couvreur, "Stimuli-responsive nanocarriers for drug delivery," *Nat. Mater.*, Vol. 12, No. 11, 991–1003, 2013.
9. Bao, J., S. Guo, X. Zu, Y. Zhuang, D. Fan, Y. Zhang, Y. Shi, Z. Ji, J. Cheng, and X. Pang, "Polypyrrole-coated magnetite vortex nanoring for hyperthermia-boosted photothermal/magnetothermal tumor ablation under photoacoustic/magnetic resonance guidance," *Front Bioeng. Biotechnol.*, Vol. 9, 721617, 2021.
10. Thirunavukkarasu, G. K., K. Cherukula, H. Lee, Y. Y. Jeong, I.-K. Park, and J. Y. Lee, "Magnetic field-inducible drug-eluting nanoparticles for image-guided thermo-chemotherapy," *Biomaterials*, Vol. 180, 240–252, 2018.
11. Feng, X. H., F. Gao, and Y. J. Zheng, "Thermally modulated photoacoustic imaging with superparamagnetic iron oxide nanoparticles," *Opt. Lett.*, Vol. 39, No. 12, 3414–3417, 2014.
12. Piao, D. Q., R. A. Towner, N. Smith, and W. R. Chen, "Magnetothermoacoustics from magnetic nanoparticles by short bursting or frequency chirped alternating magnetic field: A theoretical feasibility analysis," *Med. Phys.*, Vol. 40, No. 6, 063301, 2013.
13. Yuan, C., B. H. Qin, H. Qin, and D. Xing, "Increasing dielectric loss of a graphene oxide nanoparticle to enhance the microwave thermoacoustic imaging contrast of breast tumor," *Nanoscale*, Vol. 11, No. 46, 22222–22229, 2019.
14. Feng, X. H., F. Gao, and Y. J. Zheng, "Magnetically mediated thermoacoustic imaging toward deeper penetration," *Appl. Phys. Lett.*, Vol. 103, 083704, 2013.
15. Wen, L., S. Yang, J. Zhong, Q. Zhou, and D. Xing, "Thermoacoustic imaging and therapy guidance based on ultra-short pulsed microwave pumped thermoelastic effect induced with superparamagnetic iron oxide nanoparticles," *Theranostics*, Vol. 7, No. 7, 1976–1989, 2017.
16. Feng, X. H., F. Gao, and Y. J. Zheng, "Modulatable magnetically mediated thermoacoustic imaging with magnetic nanoparticles," *Appl. Phys. Lett.*, Vol. 106, 153702, 2015.
17. Li, Y., G. Liu, J. Song, and H. Xia, "Imaging method and experimental research on thermoacoustic imaging with current injection," *High Voltage Engineering*, Vol. 46, No. 12, 4113–4119, 2020.

18. Nan, H. and A. Arbabian, "Peak-power-limited frequency-domain microwave-induced thermoacoustic imaging for handheld diagnostic and screening tools," *IEEE Trans. Microwave Theory Tech.*, Vol. 65, No. 7, 2607–2616, 2017.
19. Daqing, P., "Magneto-thermal-acoustic differential-frequency imaging of magnetic nanoparticle with magnetic spatial localization: A theoretical prediction," *Energy Based Treatment of Tissue and Assessment IX, Proceedings of SPIE 10066*, 2017.
20. Zheng, Y., F. Gao, and X. Feng, "Electromagnetic acoustics sensing and imaging for biomedical applications," *2014 IEEE MTT-S International Microwave Workshop Series on RF and Wireless Technologies for Biomedical and Healthcare Applications (IMWS-Bio2014)*, 1–3, 2014.
21. Minghua, X. and L. V. Wang, "Time-domain reconstruction for thermoacoustic tomography in a spherical geometry," *IEEE Trans. Med. Imaging*, Vol. 21, No. 7, 814–822, 2002.
22. Liu, H., Y. Li, and G. Liu, "Thermoacoustic tomography from magnetic nanoparticles by single-pulse magnetic field," *Med. Phys.*, Vol. 49, No. 1, 521–531, 2022.
23. Gabriel, C., S. Gabriel, and E. Corthout, "The dielectric properties of biological tissues. 1. Literature survey," *Phys. Med. Biol.*, Vol. 41, No. 11, 2231–2249, 1996.
24. Li, Y., G. Liu, J. Song, and H. Xia, "Influence exerted by bone-containing target body on thermoacoustic imaging with current injection," *Chin. Phys. B*, Vol. 28, No. 4, 044302, 2019.
25. Rosensweig, R. E., "Heating magnetic fluid with alternating magnetic field," *J. Magn. Magn. Mater.*, Vol. 252, 370–374, 2002.
26. Li, Y., G. Liu, and J. Song, "Magnetically mediated thermoacoustic imaging with single coil based on non-uniform magnetic field excitation," *J. Appl. Phys.*, Vol. 128, 174901, 2020.